Packet Collision Probability of Direct-to-Satellite IoT Systems

Enrico Testi, *Member, IEEE*, and Enrico Paolini, *Senior Member, IEEE*

***Abstract*—We investigate the packet collision probability among uncoordinated devices, in the uplink of Direct-to-Satellite Internet of Things (DtS-IoT). Both the satellite spot shape and its motion along its orbital path are considered in the analysis. We analyze the probability of no uplink collision under two DtS-IoT settings: 1) unconfirmed ALOHA over a single channel, e.g., long-range wide-area network (LoRaWAN) class A with long-range chirp spread spectrum (LoRa-CSS) modulation and 2) unconfirmed ALOHA with frequency-hopping compliant with LoRaWAN class A with long-range frequency-hopping spread spectrum (LR-FHSS). A closed-form solution is derived for the former, while an upper bound is found for the latter. The analytical results are validated by comparison with the outcomes of extensive simulations, showing that the obtained closed-form expressions accurately predict the probability of no collision. Moreover, the upper bound for the frequency-hopping case is proven to be tighter when there are less than 35 hopping channels. Finally, we provide a concise performance comparison between LoRa-CSS and LR-FHSS in DtS-IoT, showing that LR-FHSS significantly increases the number of devices that can simultaneously transmit during a satellite pass, thereby enhancing uplink capacity.**

***Index Terms*—Direct-to-Satellite Internet of Things (DtS-IoT), frequency-hopping spread spectrum, Internet of Remote Things, low-Earth orbit (LEO) satellite, machine-to-machine communications.**

I. Introduction

RECENTLY, Internet of Things (IoT) services based on low-Earth orbit (LEO) satellites have received a considerable interest from private companies, international standardization bodies, and the research community [2], [3], [4], [5], [6], [7]. Although terrestrial IoT is already playing a pivotal role in the evolution of next-generation wireless networks, there still are many use cases that require a more global, scalable, adaptable, and robust solution [8]. These use cases encompass monitoring of remote areas, connecting unserved or remote regions, and facilitating intelligent global transport management. A possible solution to address these needs lies in the "Internet of space things," i.e., a network of cyber–physical systems that will enable global connectivity by exploiting satellite constellations [9], [10]. The Third Generation Partnership Project (3GPP) promotes its Narrowband IoT (NB-IoT)-based standard for nonterrestrial networks (NTNs), while numerous corporates, e.g., Lacuna Space and EchoStar Mobile, are sponsoring the use of low-power wide-area networks (LPWANs) based on proprietary technologies (e.g., Semtech ones) for Direct-to-Satellite IoT (DtS-IoT) communications [11], [12], [13], [14].

A new communication scheme, long-range frequency-hopping spread spectrum (LR-FHSS), specifically designed for long distance and low data rate uplink communications, has recently been introduced [15], [16]. In essence, LR-FHSS exploits fast frequency hopping to maintain a radio link budget equivalent to that of long-range chirp spread spectrum (LoRa-CSS) while concurrently enhancing network capacity, which makes it a serious candidate for satellite communications. Concurrently, the well-established LoRa-CSS modulation has been updated with new operating frequencies, channel bandwidths, spreading factors (SFs), and data rates, available within the Long Range Wide Area Network (LoRaWAN) specifications.

Therefore, while LR-FHSS has been specifically tailored by Semtech for satellite use cases, the newly released LoRaWAN configurations may potentially unlock new services and use cases for the well-established LoRa-CSS modulation. In light of the above-reviewed recent updates, it is not yet fully clear which technology is the most suitable for DtS-IoTcommunications. Indeed, all the aforementioned protocols have different characteristics in terms of channel access strategy and receiver sensitivity, both playing a crucial role in link availability and quality of service. In IoT systems based on LEO satellites, the end devices (EDs) on ground wait for the satellite to be reachable and then send their uplink data without coordinating with each other. As such, each ED performs a random channel access during the satellite visibility time, experiencing a collision probability that depends on the number of neighboring EDs, the adopted uncoordinated access protocol, and its connection time. In addition, LPWANs are designed to operate with low transmission powers, which makes the link budget, and thus the receiver sensitivity, a critical issue for satellite communications with such technologies. This article introduces a robust and pragmatic framework for the performance analysis of DtS-IoT systems. The outcomes of this study hold valuable implications for practical applications, offering support to DtS-IoT system dimensioning.

Received 10 May 2024; revised 9 August 2024; accepted 16 September 2024. Date of publication 30 September 2024; date of current version 9 January 2025. This work was supported by the European Union under the Italian National Recovery and Resilience Plan of NextGenerationEU, partnership on "Telecommunications of the Future" under Grant PE00000001—"RESTART." This article was presented in part at the 2024 IEEE International Symposium on Personal, Indoor and Mobile Radio Communications, Valencia, Spain. *(Corresponding author: Enrico Paolini.)*

The authors are with CNIT/WiLab, DEI, University of Bologna, 47522 Cesena, Italy (e-mail: enrico.testi@unibo.it; e.paolini@unibo.it).

Digital Object Identifier 10.1109/JIOT.2024.3470113

A. Prior Work

Since Abramson's seminal work [17], random access (namely, ALOHA and its evolution, such as, e.g., slotted, framed, spread spectrum, diversity, and collision resolution ALOHA [18], [19], [20], [21]), has always been a vibrant research topic in several application domains, including radio frequency identification (RFID) [22], IoT [23], and satellite communications [4]. In the last years, a large volume of research has been conducted to study and assess the performance of the most prominent satellite IoT technologies, mostly random access based.

In [13], various medium access protocols for satellite communications are compared in terms of throughput and energy efficiency, focusing on IoT applications and the use of CubeSats. In [24] and [25], stochastic geometry tools are employed to measure the potential benefits drones may offer in bolstering connectivity within IoT networks. Building upon these works, in [26] and [27], a stochastic geometry framework is proposed to study the connectivity between IoT devices and a constellation of LEO satellites, encompassing both direct communication and communication relayed by a terrestrial gateway. One of the most interesting outcomes of this study is that direct-to-satellite (DtS) communications result in higher coverage probability but a lower average IoT battery lifetime compared to indirect communication.

In [6], several laboratory and outdoor experiments are presented to evaluate the resilience of LoRa-CSS modulation to Doppler shifts and Doppler rates typical of LEO satellites, emphasizing its robustness for altitudes exceeding 550 km. Sparse satellite constellations for DtS-IoT are investigated in [28], where the authors show how a tradeoff between in-orbit infrastructure and latency can be achieved. A LoRa-CSS-based LEO satellite IoT scheme is proposed in [29], where a closed-form expression for the connection probability, depending on the received signal strength indicator is also derived.

Different LoRa-CSS and LR-FHSS access schemes for DtS communications are compared in [6], where a theoretical mixed integer linear programming (MILP) model that provides an upper bound on network performance is proposed. A LEO satellite IoT scheme is proposed in [29] to study the uplink performance of LoRa-CSS. Furthermore, a closed-form expression for the LoRa-CSS connection probability, depending on the received signal strength indicator under Rician fading, is derived. The authors consider a fixed satellite spot position and study the network interference assuming a Poisson-distributed number of transmitting users inside the spot.

In [30], an analytical approach is presented to derive the outage probability of an LR-FHSS satellite-based IoT network taking into account noise, channel fading impairments, and capture effect. Moreover, in [31], the packet delivery mechanisms of LR-FHSS for ground-to-LEO satellite communications are studied, developing analytical and simulation models. Works [30] and [31] assume that the interarrival times for successive packets follow an exponential distribution, and that the LR-FHSS packet fragments collision events are independent. The presented results highlight the feasibility of large-scale LR-FHSS networks and certain tradeoffs associated with the two novel data rate schemes available for the European regions. Furthermore, the investigation in [31] reveals that the primary cause of packet loss in an LR-FHSS communication link is represented by the loss of all the transmitted header replicas.

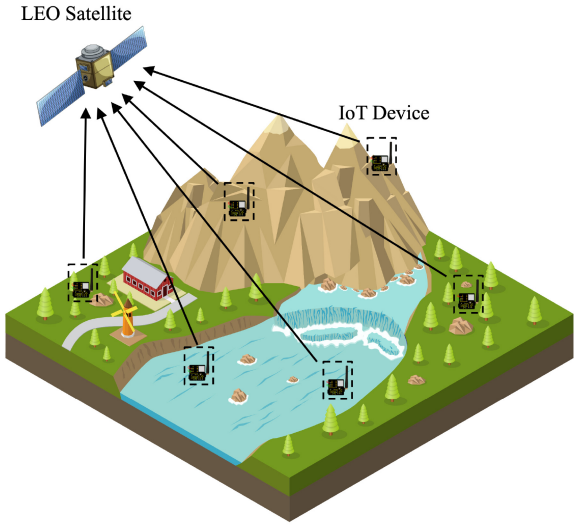

Fig. 1. Satellite IoT scenario in which a set of active devices deployed in remote areas perform DtS uplink transmissions.

B. Contribution

To the best of the authors' knowledge, so far the probability of packet collision (i.e., mutual interference) among the nodes of a DtS-IoT network adopting random access, considering the satellite motion and its effect on the statistic of the packet arrivals, has not been investigated. For example, most of the above-mentioned works assume by default that packet arrivals at the satellite follow a time Poisson process of some rate ρ [packets/s] regardless of the geometrical configuration of the coverage area (which we refer to as "satellite spot"), its motion at a certain velocity, the distribution of nodes on ground, and the limited contact time between the nodes and the satellite. However, in the scenario under analysis, each device contends to deliver its packet within its short contact time, typically spanning a few tens of seconds. Moreover, the contention windows of devices located in the same geographic area, thus potentially interfering with each other, may be misaligned and have different sizes depending on their positions with respect to the spot trajectory. Therefore, in this article, we first formulate a contention-based problem that captures the above-mentioned features of a DtS-IoT system based on random access; then, we derive the analytical expression of the probability of no uplink collision for unconfirmed ALOHA over a single channel (representing, e.g., LoRaWAN class A with LoRa-CSS modulation) and an upper bound on the same probability for unconfirmed ALOHA with frequency-hopping compliant with LR-FHSS. In the process we show that, if users on ground are distributed according to a Poisson point process (PPP), the steady-state packet arrival process is indeed Poisson, and we obtain the explicit expression of the rate ρ as

a function of the system parameters. The obtained closed-form solutions can be used to estimate the maximum number of IoT devices that can be served during the satellite pass ensuring a desired probability of no uplink collision.

The main contributions are summarized as follows.

1) Considering a DtS-IoT system, we derive the analytical expression of the probability of no uplink collision for unconfirmed ALOHA over a single channel and an upper bound on the same probability for unconfirmed ALOHA with frequency-hopping compliant with LR-FHSS. The expressions reveal the explicit dependence on system parameters as the satellite velocity, the spot size, the node density on ground, and the packet time-on-air.
2) We obtain the upper bound in the LR-FHSS case removing the assumptions that packet fragment collision events are independent.
3) We reveal that the obtained expressions are independent of the satellite spot shape, provided that it belongs to a specific set of shapes with certain properties.
4) We validate the analytical models through a comparison with the results obtained by Monte Carlo simulations. The upper bound reveals to be tight under certain conditions.

This article is organized as follows. Section II introduces the scenario and system model. Sections III and IV present the analysis for unconfirmed ALOHA over a single channel and with LR-FHSS, respectively. Considerations on the per-user packet decoding error probability are exposed in Section V. Numerical results are presented in Section VI. Conclusions are drawn in Section VII. This article was presented in part at the 2024 IEEE International Symposium on Personal, Indoor and Mobile Radio Communications [1].

Notation: Boldface and plain lower case letters denote vectors and scalars, respectively. The modulus of vector $\boldsymbol{a}$ is denoted by $|\boldsymbol{a}|$. The interval between reals a and b, endpoints included, is indicated as $[a, b]$. The operations $\mathsf{A} \cup \mathsf{B}$ and $\mathsf{A} \cap \mathsf{B}$ denote the union and the intersection of the events A and B, respectively. The uniform distribution in the interval $[a, b]$ is denoted by $\mathcal{U}(a, b)$. We let $\lceil \cdot \rceil$ be the ceiling operator. Hereafter, "success" refers to the event of no uplink collision. The specific definition of a success event, in each of the two analyzed DtS-IoT settings, is addressed at the beginning of Sections III and IV, respectively.

II. System Model

We consider the uplink of a nonterrestrial IoT system in which devices on ground, hereafter also referred to as "users" or "nodes," contend to transmit packets to a LEO satellite during its pass. The reference scenario is illustrated in Fig. 1. The satellite moves, parallel to the ground, with a constant velocity $\boldsymbol{v}$ such that $v = |\boldsymbol{v}|$. At every pass, each active node attempts transmission of one packet. We assume that all packets have the same transmission/reception time T, also referred to as the packet "time-on-air." By Time of Arrival (ToA) of a packet we mean the start time of packet reception at the satellite; this equals the packet transmission start time plus the propagation time. We assume the existence of a downlink channel through which the satellite periodically broadcasts its updated orbital data to the nodes. This way, each node is aware of the start and end of the pass and can adjust the start time of its transmission to enforce a desired ToA of its packet at the satellite.

Definition 1 (Valid ToA Range): The valid ToA range of a packet is the interval of ToA values such that the packet is entirely received within the satellite pass, so that the onboard satellite receiver is potentially able to demodulate and decode it. The size of the valid ToA range equals the node-satellite contact time minus the packet transmission time.

The access protocol falls into the class of unconfirmed ALOHA protocols, i.e., unslotted ALOHA without acknowledgment messages, and works as follows. During the pass, the generic node sets the ToA of its packet by drawing a random variable uniformly distributed in the valid ToA range and starts its transmission accordingly. As such, transmissions from different nodes in the same area are asynchronous. The access protocol is uncoordinated, meaning that users act independently of each other with no coordination.

Since the shape of the satellite spot on Earth depends on the type and the number of onboard antennas, we identify a set of spot shapes for which the developed analysis is valid. We refer to it as the set of target spot shapes. Throughout this article, we neglect the Earth curvature, modeling the ground as a plane, and we assume that the satellite spot shape does not change over time.

Definition 2 (Target Spot Shape): A satellite spot shape is called a target one when: 1) it is convex and 2) it exhibits line symmetry about a line ℓ_1 and about a second line ℓ_2 orthogonal to ℓ_1.

Examples of target spot shapes (regardless of their practical feasibility) are the square, the circle, and the ellipse. The analysis is carried out considering a single satellite pass and using a Cartesian coordinate system such that the symmetry line ℓ_2 coincides with the y-axis and the satellite velocity $\boldsymbol{v}$ is parallel to ℓ_2. Without loss of generality, we assume that time $t = 0$ corresponds to the time at which the symmetry line ℓ_1 overlaps with the x-axis. Letting $\mathcal{S}(t) \subset \mathbb{R}^2$ be the satellite spot at time t and $\partial\mathcal{S}(t)$ be its boundary,[1] the above choice allows us to define the time-independent parameter

$$L = \max\{x : (x, y) \in \partial\mathcal{S}(t)\}. \tag{1}$$

The analysis is performed considering a reference node for which a valid ToA range exists. Without loss of generality, the reference node is in position $(a, 0)$, for some a such that $-L < a < L$. We denote by $\mathcal{R} \in \mathbb{R}^2$ the region, with boundary $\partial\mathcal{R}$ and area $A_{\mathcal{R}}$, that is swept by the satellite spot during the contact time with the reference node. An example is illustrated in Fig. 2. Note that another device can potentially interfere the reference one only if its spatial position belongs to region $\mathcal{R}$. The potential interferers of the reference node are assumed to be scattered in the x–y plane according to a PPP with spatial density λ, such that their number N in a measurable region is a Poisson distributed random variable.

[1] $\partial\mathcal{S}$ represents the boundary of the projection of the satellite's footprint onto the ground. For instance, if the footprint has a circular shape, $\partial\mathcal{S}$ denotes its circumference.

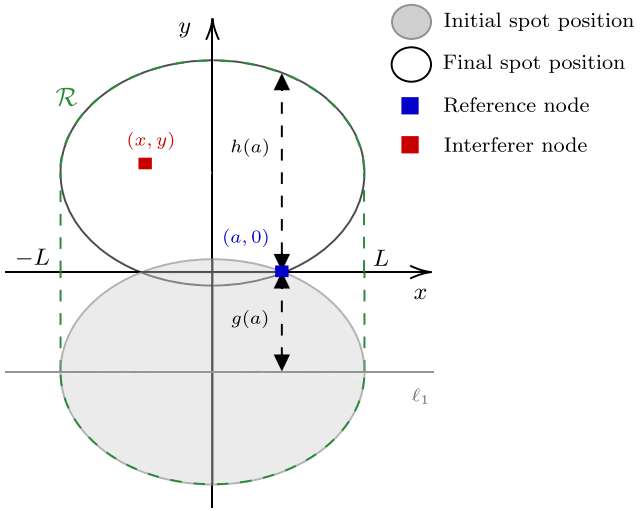

Fig. 2. Illustration of the region $\mathcal{R}$ defined by the translation of the satellite spot along the positive y-axis direction for a generic target spot shape. At time $t = 0$, the center of the spot corresponds to the origin.

If a node is in position (x, y) then, with the above choice of the $t = 0$ time, the valid ToA range of its packet is the interval

$$W_{\text{ToA}}(x, y, T) = \left[\frac{y - g(x)}{v}, \frac{y + g(x)}{v} - T\right] \tag{2}$$

where $g(x) > 0$ is an invertible function of the node abscissa and depends on the spot shape. An example for the circular spot shape is $g(x) = \sqrt{L^2 - x^2}$. In order for the contact time of a node to be sufficient for the transmission of one packet, we must have $2g(x)/v - T \geq T$, a condition that is verified if and only if

$$g(x) \geq vT. \tag{3}$$

Thus, from (3), the range of the abscissa of the reference node is reduced to $-a_{\max} \leq a \leq a_{\max}$ where $a_{\max} = |g^{-1}(vT)|$. We also define $h(x) > 0$ as the positive ordinate such that $(x, h(x)) \in \partial\mathcal{R}$, noting that $h(x) = g(0) + g(x)$. An example for the circular spot shape is $h(x) = L + \sqrt{L^2 - x^2}$.

III. Probability of No Uplink Collision Over Single-Frequency Channel

In this section, we assume that, during the satellite pass, active nodes transmit their packets asynchronously over the same frequency channel through the unconfirmed ALOHA protocol introduced in Section II. Although the main result, expressed by Theorem 1 below, is valid regardless of the specific modulation, numerical results in Section VI will target LoRaWAN class A with LoRa-CSS modulation. We denote by S the event of no uplink collision, i.e., the event that no portion of the packet transmitted by the reference user is affected by interference, and we develop an analytical expression of the probability $P(\mathsf{S})$. The obtained closed-form expression is valid for any spot shape belonging to the target spot shape set.

Theorem 1: Let the satellite spot shape be a target one and, during the satellite pass, each node on ground transmit one uplink packet over a single-frequency asynchronous channel. Then, the probability that no portion of the packet transmitted by the generic node is interfered, $P(\mathsf{S})$, is given by

$$P(\mathsf{S}) = e^{-4LTv\lambda}. \tag{4}$$

Proof: Let N be the number of potential interferers of the reference user in the region $\mathcal{R}$ and τ_{ref} be the ToA of the reference packet. Recalling that the area of $\mathcal{R}$ is $A_{\mathcal{R}}$, the probability $P(\mathsf{S})$ can be developed as

$$\begin{aligned} P(\mathsf{S}) &= \sum_{n=0}^{\infty} P(N = n) P(\mathsf{S}|n) \\ &= \sum_{n=0}^{\infty} \frac{(A_{\mathcal{R}}\lambda)^n}{n!} e^{-A_{\mathcal{R}}\lambda} P(\mathsf{S}|n) \\ &\overset{\text{(a)}}{=} \frac{e^{-A_{\mathcal{R}}\lambda}}{2g(a)/v - T} \\ &\quad \cdot \sum_{n=0}^{\infty} \frac{(A_{\mathcal{R}}\lambda)^n}{n!} \int_{-g(a)/v}^{g(a)/v - T} P(\mathsf{S}|n, \tau_{\text{ref}})\, \mathrm{d}\tau_{\text{ref}} \end{aligned} \tag{5}$$

where (a) is due to τ_{ref} being uniformly distributed in $W_{\text{ToA}}(a, 0, T)$. This latter interval is given by (2) with $x = a$ and $y = 0$. Next, given that in $\mathcal{R}$ there are n potential interferers of the reference node, we have $\mathsf{S} = \mathsf{S}_1 \cap \ldots \cap \mathsf{S}_n$, where S_i is the event that the packet of the reference node is not interfered by the one of node i. Since any two events S_i and S_j, $i \neq j$, are independent and $P(\mathsf{S}_i|n,\ \tau_{\text{ref}}) = P(\mathsf{S}_j|n,\ \tau_{\text{ref}})$ we can recast (5) as

$$\begin{aligned} P(\mathsf{S}) &= \frac{e^{-A_{\mathcal{R}}\lambda}}{2g(a)/v - T} \\ &\quad \cdot \sum_{n=0}^{\infty} \frac{(A_{\mathcal{R}}\lambda)^n}{n!} \int_{-g(a)/v}^{g(a)/v - T} \left[P(\mathsf{S}_1|n, \tau_{\text{ref}})\right]^n \mathrm{d}\ \tau_{\text{ref}}. \end{aligned} \tag{7}$$

Let $\mathsf{C}_1 = \bar{\mathsf{S}}_1$ be the event that the packet transmitted by node 1 has a time overlap with that of the reference node.

Recall that the potential interferers' spatial positions follow a PPP so that, given that there are n of them in $\mathcal{R}$, the position of each of them is uniformly distributed in $\mathcal{R}$. Then, for any target spot shape (Definition 2), we can write

$$\begin{aligned} P(\mathsf{C}_1|n, \tau_{\text{ref}}) &= \int_{\mathbb{R}^2} P(\mathsf{C}_1|n, \tau_{\text{ref}}, x, y) f_{X,Y}(x, y)\, \mathrm{d}x\mathrm{d}y \\ &= \frac{1}{A_{\mathcal{R}}} \int_{\mathcal{R}} P(\mathsf{C}_1|n, \tau_{\text{ref}}, x, y)\, \mathrm{d}x\mathrm{d}y \\ &= \frac{1}{A_{\mathcal{R}}} \int_{\mathcal{R}} P(\mathsf{C}_1|\tau_{\text{ref}}, x, y)\, \mathrm{d}x\mathrm{d}y \end{aligned} \tag{8}$$

where $f_{X,Y}(x, y)$ is the probability density function (PDF) of the position of node 1; given that there are n potential interferers, it is equal to $1/A_{\mathcal{R}}$ for all $(x, y) \in \mathcal{R}$ and is null elsewhere. Note that conditioning on n can be omitted after specifying $f_{X,Y}(x, y)$.

Next, let us partition the interval $[-L, L]$ on the x-axis into $2L/\Delta x$ smaller intervals, each of size Δx. Let x_i be the center of the ith such interval and $\mathcal{R}_i$ be the rectangular region

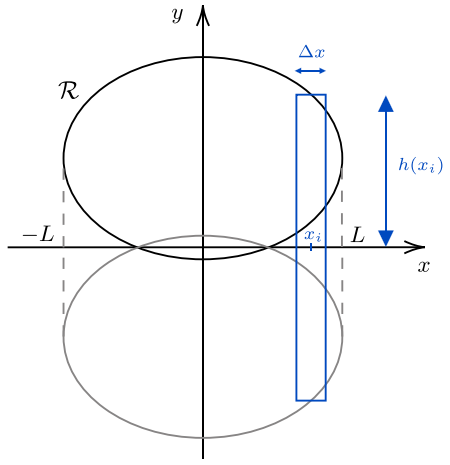

Fig. 3. Approximation of the region $\mathcal{R}$ swept by the satellite (during the contact time with the reference node) as the union of rectangular regions.

$[(i-1)\Delta x, i\Delta x] \times [-h(x_i), h(x_i)]$. This is depicted in Fig. 3. Then, we can write

$$P(\mathsf{C}_1|n,\tau_{\text{ref}}) = \frac{1}{A_{\mathcal{R}}} \cdot \lim_{\Delta x\to 0} \sum_{i=1}^{2L/\Delta x} \int_{(i-1)\Delta x}^{i\Delta x} \int_{-h(x_i)}^{h(x_i)} P(\mathsf{C}_1|\tau_{\text{ref}},x_i,y)\,\mathrm{d}y\mathrm{d}x. \quad (9)$$

The probability $P(\mathsf{C}_1|\ \tau_{\text{ref}},x_i,y)$ can be obtained observing that it is the probability that the ToA of the interfering packet from a node in position (x_i,y) falls between $\tau_{\text{ref}}-T$ and $\tau_{\text{ref}}+T$, i.e., in the vulnerability time interval of the reference packet. Using the fact that the ToA of the interfering packet is uniformly distributed in $W_{\text{ToA}}(x_i,y,T)$ we obtain (6), shown at the bottom of the page. Regarded as a function of y, $P(\mathsf{C}_1|\ \tau_{\text{ref}},x_i,y)$ has therefore a trapezoidal shape. It is immediate to verify that the area of the trapezoid is $2Tv$. We then have

$$\int_{-h(x_i)}^{h(x_i)} P(\mathsf{C}_1|\tau_{\text{ref}},x_i,y)\,\mathrm{d}y = 2Tv. \quad (10)$$

Incorporating (10) into (9), we obtain

$$P(\mathsf{C}_1|n,\tau_{\text{ref}}) = \frac{1}{A_{\mathcal{R}}} \lim_{\Delta x\to 0} \sum_{i=1}^{2L/\Delta x} \int_{(i-1)\Delta x}^{i\Delta x} 2Tv\,\mathrm{d}x = \frac{4LTv}{A_{\mathcal{R}}}. \quad (11)$$

Using the fact that $P(\mathsf{S}_1|n,\tau_{\text{ref}}) = 1 - P(\mathsf{C}_1|n,\tau_{\text{ref}})$ and substituting into (7) yields the final expression

$$P(\mathsf{S}) = e^{-A_{\mathcal{R}}\lambda} \sum_{n=0}^{\infty} \frac{1}{n!}\left[A_{\mathcal{R}}\lambda\left(1-\frac{4LTv}{A_{\mathcal{R}}}\right)\right]^n = e^{-4LTv\lambda}. \quad (12)$$

The proof is completed by observing that, in (10), the whole area below the trapezoidal-shaped function (equal to $2Tv$) must be taken since the integration interval $[-h(x_i), h(x_i)]$ includes the major base of the trapezoid, that coincides with the interval $[\tau_{\text{ref}}v-g(x_i),\ (\tau_{\text{ref}}+T)v+g(x_i)]$ from (6). This fact immediately follows from $\tau_{\text{ref}} \geq -g(0)/v$ and $\tau_{\text{ref}} \leq g(0)/v - T$, since $h(x_i) = g(0) + g(x_i)$. ■

Remark 1: In case *B*, orthogonal frequency channels are available and each node chooses one uniformly at random, Theorem 1 remains valid upon replacing λ with λ/B (on invoking independent thinning of Poisson processes).

Remark 2: While the contact time of the reference node depends on a, the probability $P(\mathsf{S})$ does not. This is because smaller or larger contact times correspond to smaller or larger areas $A_{\mathcal{R}}$, decreasing or increasing the average number of potential interferers, respectively.

An alternative proof of Theorem 1 can be developed by analyzing the packet arrival process at the satellite. This alternative proof is proposed in Appendix B, where it is shown that if users on ground are distributed according to a PPP and the satellite spot does not initially contain any node, then the packet arrival process is an inhomogeneous Poisson process whose rate converges to a constant value $\rho = 2Lv\lambda$ [packets/s].

IV. Extension to LR-FHSS Protocol

In this section, we extend the analysis to an unconfirmed ALOHA protocol with frequency hopping that captures the essential features of LR-FHSS, a new scheme based on frequency-hopping spread spectrum and regarded as the "satellite counterpart" of LoRa-CSS. It features an intraframe frequency-hopping scheme with the goal of achieving better sensitivity, interference rejection, and uplink capacity with respect to traditional IoT modulation schemes [15], [16]. The LR-FHSS payload is preceded by a header. The header is replicated N_H times, where $N_H \in \{2,3\}$, and each replica is sent over a specific occupied bandwidth (OBW), i.e., a different frequency subchannel. In the context of LR-FHSS we denote by τ_{ref} the ToA of the first header replica of the reference device, referring to it simply as the reference device ToA. The header has fixed duration T_H, and at least one of its replicas needs to be correctly received to properly demodulate the payload. The payload is split into N_F fragments, all with the same time duration T_F; each fragment is transmitted over a specific OBW. The sequence of OBWs used for the

$$P(\mathsf{C}_1|\ \tau_{\text{ref}},x_i,y) = \begin{cases} 0, & \text{if } y < \tau_{\text{ref}}\,v - g(x_i) \\ \frac{y+g(x_i)-\tau_{\text{ref}}v}{2g(x_i)-Tv}, & \text{if } \tau_{\text{ref}}\,v - g(x_i) \leq y < (\tau_{\text{ref}}+2T)v - g(x_i) \\ \frac{2Tv}{2g(x_i)-Tv}, & \text{if } (\tau_{\text{ref}}+2T)v - g(x_i) \leq y < (\tau_{\text{ref}}-T)v + g(x_i) \\ \frac{(\tau_{\text{ref}}+T)v-y+g(x_i)}{2g(x_i)-Tv}, & \text{if } (\tau_{\text{ref}}-T)v + g(x_i) \leq y < (\tau_{\text{ref}}+T)v + g(x_i) \\ 0, & \text{if } y \geq (\tau_{\text{ref}}+T)v + g(x_i) \end{cases} \quad (6)$$

transmission of header replicas and fragments is generated randomly. The scheme is structured in such a way that a user packet is successfully received when so are at least one copy of the header and γ payload fragments. The ideal value of γ is $\gamma = \lceil N_F \cdot \mathrm{CR} \rceil$, where CR is the code rate of the channel code protecting the payload. However, in practice, the number of fragments that must be received for a successful packet transmission has to be slightly higher.

Let B be the number of available OBW for frequency hopping, and $\mathsf{C}_{\mathrm{H}_j}$ be the event that replica j of the header of the reference device is (even partially) interfered by a header replica or a payload fragment of another device. Moreover, let $\mathsf{S}_{i\mathrm{H}}$ be the event that a header replica of the reference node is not interfered by potential interferer i, i.e., by none of its header replicas or payload fragments. We remark that any two events $\mathsf{S}_{i\mathrm{H}}$ and $\mathsf{S}_{j\mathrm{H}}$, $i \neq j$, are independent and that $P(\mathsf{S}_{i\mathrm{H}}|n,\ \tau_{\mathrm{ref}}) = P(\mathsf{S}_{j\mathrm{H}}|n,\ \tau_{\mathrm{ref}})$, n being the number of potential interferers.

We now analyze the probability that at least one header replica and at least γ payload fragments of the packet, transmitted by any node under LR-FHSS protocol, are not affected by interference when the satellite spot shape belongs to the target spot shape set. We denote this event by S and refer to it as "no uplink collision" event.

Theorem 2: Let the satellite spot shape be a target one and, during the satellite pass, each node on ground transmit one uplink packet adopting the LR-FHSS scheme. Let α be such that $P(\mathsf{S}_{i\mathrm{H}}|n, \tau_{\mathrm{ref}}) \leq \alpha$ for all i. Moreover, let

$$P\Big(\bigcap_{j=1}^{N_H} \mathsf{C}_{\mathrm{H}_j}|n, \tau_{\mathrm{ref}}\Big) \geq \prod_{j=1}^{N_H} P\big(\mathsf{C}_{\mathrm{H}_j}|n, \tau_{\mathrm{ref}}\big). \tag{14}$$

Then, the probability of no uplink collision for the packet transmitted by the generic active node is upper bounded by (13), shown at the bottom of the page.

Remark 3: Inequality (14) represents the positive association between the interference events, i.e., $P(\mathsf{C}_{\mathrm{H}_j}|\mathsf{C}_{\mathrm{H}_{j-1}}, \ldots, \mathsf{C}_{\mathrm{H}_1}) \geq P(\mathsf{C}_{\mathrm{H}_j})$ for $1 < j \leq N_H$. For the sake of clarity, this hypothesis means that the event of interference of header j increases the interference probability of header $j+1$. Intuitively, this comes from the fact that the vulnerability time windows of the two headers are partially overlapped. However, we show that this assumption holds by numerical simulations reported in Fig. 5 of Section VI.

Proof: Using the same notation adopted in Theorem 1, the expression (5) for $P(\mathsf{S})$ remains valid upon redefining T as $T = N_H T_H + N_F T_F$. The probability of no interference, given that there are n potential interferers and that τ_{ref} is the reference device ToA, is expressed as

$$P\big(\mathsf{S}|n, \tau_{\mathrm{ref}}\big) = P(S_{\mathrm{H}}|n, \tau_{\mathrm{ref}}) P\big(S_{\gamma\mathrm{F}}|n, \tau_{\mathrm{ref}}\big) \tag{15}$$

where $P(\mathsf{S}_{\mathrm{H}}|n, \tau_{\mathrm{ref}})$ is the probability that at least one of the N_H header replicas is not interfered, and $P(\mathsf{S}_{\gamma\mathrm{F}}|n, \tau_{\mathrm{ref}})$ is the probability that at least γ payload fragments are not interfered. The probability of no interference of at least one of the N_H header replicas is

$$\begin{aligned} P\big(\mathsf{S}_{\mathrm{H}}|n, \tau_{\mathrm{ref}}\big) &= 1 - P\Big(\bigcap_{j=1}^{N_H} \mathsf{C}_{\mathrm{H}_j}|n, \tau_{\mathrm{ref}}\Big) \\ &\overset{(a)}{\leq} 1 - \prod_{j=1}^{N_H} P\Big(\mathsf{C}_{\mathrm{H}_j}|n, \tau_{\mathrm{ref}}\Big) \\ &= 1 - \Big(1 - P\big(\mathsf{S}_{i\mathrm{H}}|n, \tau_{\mathrm{ref}}\big)^n\Big)^{N_H} \end{aligned} \tag{16}$$

where (a) follows directly from (14). We now substitute $P(\mathsf{S}_{i\mathrm{H}}|n, \tau_{\mathrm{ref}})$ in (16) with the upper bound α, obtaining

$$P\big(\mathsf{S}_{\mathrm{H}}|n, \tau_{\mathrm{ref}}\big) \leq 1 - \Big(1 - \alpha^n\Big)^{N_H}. \tag{17}$$

Now, we can upper bound (15) as

$$\begin{aligned} P\big(\mathsf{S}|n, \tau_{\mathrm{ref}}\big) &\leq P\big(\mathsf{S}_{\mathrm{H}}|n, \tau_{\mathrm{ref}}\big) \\ &\leq 1 - \Big(1 - \alpha^n\Big)^{N_H}. \end{aligned} \tag{18}$$

We now incorporate (18) in (5) and obtain (13) for $N_H = 2$ and $N_H = 3$, completing the proof. ∎

Remark 4: Let us remark that it has been shown how, since LR-FHSS applies convolutional channel coding to the payload fragments and adopts frequency hopping, $P(\mathsf{S}_{\mathrm{H}}|n, \tau_{\mathrm{ref}})$ is the driving factor in (15) [31].

In the next theorem, we derive a possible value of the upper bound α which can be used in (13). Let us define Y_j as the event that the reference header is interfered by a header (i.e., $1 \leq j \leq N_H$) or a fragment (i.e., $N_H + 1 \leq j \leq N_H + N_F$) of the generic interferer, and $N = N_H + N_F$.

Theorem 3: Let the satellite spot shape be a target one and, during the satellite pass, each node on ground transmit one uplink packet adopting LR-FHSS scheme. Then, we have

$$\begin{aligned} P\big(\mathsf{S}_{i\mathrm{H}}|n, \tau_{\mathrm{ref}}\big) \leq 1 &- \frac{\theta S_1^2}{(2-\theta)S_1 + 2S_2} \\ &- \frac{(1-\theta)S_1^2}{(1-\theta)S_1 + 2S_2} \end{aligned} \tag{19}$$

where

$$S_1 = \frac{2\nu L(T_H(2N_H + N_F) + T_F N_F)}{A_{\mathcal{R}} B} \tag{20}$$

$$S_2 = \frac{2\nu L}{A_{\mathcal{R}} B^2}\Big(T_H(N_H + 2N_F - 3) + T_F(5 - 3N_F)\Big) \tag{21}$$

$$\theta = 2\frac{S_2}{S_1} - \left\lfloor \frac{2S_2}{S_1} \right\rfloor. \tag{22}$$

$$P(\mathsf{S}) \leq \begin{cases} e^{-A_{\mathcal{R}}\lambda}\Big(-e^{A_{\mathcal{R}}\lambda\alpha^2} + 2e^{A_{\mathcal{R}}\lambda\alpha}\Big), & \text{if } N_H = 2 \\ e^{-A_{\mathcal{R}}\lambda}\Big(e^{A_{\mathcal{R}}\lambda\alpha^3} - 3e^{A_{\mathcal{R}}\lambda\alpha^2} + 3e^{A_{\mathcal{R}}\lambda\alpha}\Big), & \text{if } N_H = 3 \end{cases} \tag{13}$$

Proof: Let us express $P(\mathsf{S}_{i\mathrm{H}}|n, \tau_{\mathrm{ref}})$ as

$$P(\mathsf{S}_{i\mathrm{H}}|n, \tau_{\mathrm{ref}}) = 1 - P\left(\bigcup_{j=1}^{N} \mathsf{Y}_j|n, \tau_{\mathrm{ref}}\right) \leq 1 - \frac{\theta S_1^2}{(2-\theta)S_1 + 2S_2} - \frac{(1-\theta)S_1^2}{(1-\theta)S_1 + 2S_2} \tag{23}$$

where the inequality follows from Dawson–Sankoff lower bound on the probability of union of the events [32], [33]; the lower bound exploits S_1 and S_2 defined as

$$S_1 = \sum_{j=1}^{N} P(\mathsf{Y}_j|n, \ \tau_{\mathrm{ref}}) \tag{24}$$

and

$$S_2 = \sum_{1 \leq j < k \leq N} P(\mathsf{Y}_j \cap \mathsf{Y}_k|n, \ \tau_{\mathrm{ref}}). \tag{25}$$

The probability $P(\mathsf{Y}_j|n, \tau_{\mathrm{ref}})$ can be expressed as

$$P(\mathsf{Y}_j|n, \tau_{\mathrm{ref}}) = \frac{1}{A_{\mathcal{R}} B} \int_{\mathcal{R}} P(\mathsf{Y}_j|n, \tau_{\mathrm{ref}}, x, y) \, \mathrm{d}x\mathrm{d}y. \tag{26}$$

To develop the right-hand side of (26) for a target spot shape we can use the same procedure described in Section III. The function $f_{\mathsf{Y}_j|n,\tau_{\mathrm{ref}}}(x_i, y) = P(\mathsf{Y}_j|n, \tau_{\mathrm{ref}}, x_i, y)$ can be obtained observing that it represents the probability that the ToA of the interfering header or fragment falls in the vulnerability time interval of the header replica transmitted by the reference node. Repeating the same procedure that led to (11) in Section III, we directly obtain

$$P(\mathsf{Y}_j|n, \tau_{\mathrm{ref}}) = \begin{cases} \frac{4vLT_H}{A_{\mathcal{R}} B}, & \text{if } 1 \leq j \leq N_H \\ \frac{2vL(T_H+T_F)}{A_{\mathcal{R}} B}, & \text{if } N_H + 1 \leq j \leq N. \end{cases} \tag{27}$$

The result in (27) can be incorporated into (24) yielding (20). The probability $P(\mathsf{Y}_j \cap \mathsf{Y}_k|n, \tau_{\mathrm{ref}})$ can be calculated as in (6) but considering a reduced vulnerability time interval corresponding to the time for which the two headers or fragments (or a header and a fragment), j and k, are both overlapped in time with the reference header. Moreover, the event $\mathsf{Y}_j \cap \mathsf{Y}_k$ implies that the two fragments or headers are transmitted in the same frequency channel as the reference header. We have

$$P(\mathsf{Y}_j \cap \mathsf{Y}_{j+1}|n, \tau_{\mathrm{ref}}) = \frac{2vLT_H}{A_{\mathcal{R}} B^2} \quad \forall \, 1 \leq j < N \tag{28}$$

$$P(\mathsf{Y}_j \cap \mathsf{Y}_{j+2}|n, \tau_{\mathrm{ref}}) = \frac{2vL(T_H - T_F)}{A_{\mathcal{R}} B^2} \quad \forall \, N_H \leq j < N - 1 \tag{29}$$

and

$$P(\mathsf{Y}_j \cap \mathsf{Y}_{j+3}|n, \tau_{\mathrm{ref}}) = \frac{2vL(T_H - 2T_F)}{A_{\mathcal{R}} B^2} \quad \forall \, N_H \leq j < N - 2. \tag{30}$$

Moreover, $P(\mathsf{Y}_j \cap \mathsf{Y}_k|n, \tau_{\mathrm{ref}}) = 0$ in all cases not covered by (28)–(30); this is due to the fact that the probability of simultaneous interference from two fragments or headers that are far apart of a time interval larger than T_H is zero. Substituting (28)–(30) into (25), we obtain (21), which completes the proof. ■

V. Upper Bound on the Per-User Packet Loss Probability

Let E be the event that the packet transmitted by the reference node during its contact time is not correctly demodulated and decoded, so that the corresponding message is not received. The probability $P(\mathsf{E})$ represents the per-user packet loss probability. Moreover, let S be the event of no uplink collision, as defined at the beginning of Sections III and IV, and $\mathsf{C} = \bar{\mathsf{S}}$. Using $P(\mathsf{S})$, we can develop a general upper bound on $P(\mathsf{E})$ as

$$P(\mathsf{E}) = P(\mathsf{E}|\mathsf{C})P(\mathsf{C}) + P(\mathsf{E}|\mathsf{S})P(\mathsf{S}) \leq P(\mathsf{C}) + P(\mathsf{E}|\mathsf{S})P(\mathsf{S}) = 1 - P(\mathsf{S})\big(1 - P(\mathsf{E}|\mathsf{S})\big) \tag{31}$$

where $P(\mathsf{E}|\mathsf{S})$ is the probability that a packet is not correctly demodulated and decoded in absence of uplink collision. This latter probability, which depends on the adopted coding and modulation scheme, is due to thermal noise, Doppler shift, and Doppler rate. The bound assumes that a packet suffering from a collision is never correctly received. Concerning the probability $P(\mathsf{S})$, the exact expression (4) can be used over a single-frequency channel, while the upper bound (13) can be adopted in case of LR-FHSS protocol.

A simple channel model, often adopted to study random access, is the collision channel. We may define an "asynchronous single-frequency collision channel" as a channel where: if the reception time interval of a packet has no overlap with that of any other packet, then the packet is always correctly received; if the reception time intervals of multiple packets overlap with each other, then none of them is correctly received regardless of their interfered portions. Letting a packet slice be a header or a fragment, we may also define an "asynchronous frequency-hopping collision channel" as a channel where: if the reception time interval of a slice has no overlap with that of any other slice transmitted over the same frequency channel, then the slice is always correctly received; if the reception time intervals of multiple slices overlap with each other over the same frequency channel, then none of them is correctly received regardless of their interfered portions. Over these simple asynchronous collision channel models, we have $P(\mathsf{E}|\mathsf{S}) = 0$ and $P(\mathsf{E}|\mathsf{C}) = 1$, hence

$$P(\mathsf{E}) = 1 - P(\mathsf{S}). \tag{32}$$

For this reason, throughout this article, we have sometimes referred to $P(\mathsf{S})$ as the "success probability."

In Appendix A, Theorem 1 is used to obtain a closed-form expression for the system sum-rate over the asynchronous single-frequency collision channel. Sum-rate optimization is also discussed.

VI. Numerical Results

In this section, the validity of the proposed analytical models is first assessed. Then, the proposed models are employed to compare LoRa-CSS and LR-FHSS schemes in terms of the reliability versus scalability tradeoff. Validation of the analytical models was carried out by developing a Monte Carlo

simulator for DtS IoT communications, which is available in [34]. The tool simulates random channel access by nodes distributed on ground willing to send a message to the satellite during its pass and employing either unconfirmed ALOHA over a single channel (covering LoRaWAN class A with LoRa-CSS modulation) or unconfirmed ALOHA with frequency-hopping compliant with LR-FHSS. The satellite's pass over a reference node is simulated according to the model detailed in Section II. At each Monte Carlo iteration, the number of interferers inside the region $\mathcal{R}$ spanned by the satellite during its contact with the reference node (see Fig. 2) is drawn from a Poisson distribution with density λ; given their number, the interferers are deployed according to a uniform distribution in $\mathcal{R}$. The simulator does not assume a Poisson packet arrival process; rather, it assumes that nodes are distributed on ground according to a PPP. For different device spatial distributions, the analysis would need to be adjusted to align with the selected distribution. Our work offers a general framework that can be adapted to various node distributions, making it applicable to typical IoT scenarios.

A. Simulation Parameters

All tests were carried out considering that each node transmits a data payload of PL = 58 bytes, unless otherwise specified. Since the results of Section III apply to a LoRaWAN class A network that adopts LoRa-CSS modulation (although they are not limited to it), we considered a time-on-air for the uplink packets equal to the one of a LoRaWAN frame containing PL payload data bytes, evaluated as follows. According to [35], a specific frame format is used by LoRa-CSS devices to accommodate data: a LoRa-CSS frame begins with a preamble, that consists of a configurable number of pure upchirps, whose frequency linearly increases from $f_0-(\mathrm{BW}/2)$ to $f_0+(\mathrm{BW}/2)$, being f_0 the carrier frequency and BW the bandwidth, followed by two and a quarter downchirps, and, optionally, a frame header. The remainder of the frame includes the payload with, possibly, the corresponding CRC.

The total time-on-air of a LoRa-CSS frame depends on the combination of SF, coding rate, and bandwidth. The symbol time, i.e., the duration of a single chirp, is defined as

$$T_{\mathrm{sym}}=\frac{2^{\mathrm{SF}}}{\mathrm{BW}}. \tag{33}$$

The number of symbols composing the payload is given by

$$n_{\mathrm{pay}}=8+\max\left\{\left\lceil\frac{8\mathrm{PL}-4\mathrm{SF}+16\mathrm{CRC}+20\mathrm{H}+8}{4(\mathrm{SF}-2\,\mathrm{DE})}\right\rceil(R+4),0\right\} \tag{34}$$

where PL is measured in bytes, CRC = 1 if the CRC is used and CRC = 0 otherwise, $H=1$ when the header is enabled (i.e., explicit mode) and $H=0$ otherwise, DE = 1 when the low data rate optimization mode is enabled and DE = 0 otherwise, $R\in\{1,2,3,4\}$ is the coding rate parameter ($R=x$ corresponds to x redundancy bit every 4 data bits). Finally, the total time-on-air of a LoRa-CSS frame is given by

$$T=\left(n_{\mathrm{pre}}+\beta+n_{\mathrm{pay}}\right)T_{\mathrm{sym}} \tag{35}$$

TABLE I
SIMULATION PARAMETERS

Parameters	Values
Satellite orbit height (h)	600 km
Minimum elevation angle (ϵ)	55 °
Satellite velocity (v)	7.5 km/s
Spot shape parameter (L)	420.124 km
Payload size (PL)	58, 100 bytes
H	1
CRC	1
β	4.25
LoRa code rate (R)	1
LoRa bandwidth (BW)	125 kHz
LoRa spreading factor (SF)	7, 10
OBW Channels (B)	35, 60, 86
Header replicas (N_{H})	2 (CR 2/3), 3 (CR 1/3)
Header duration (T_{H})	233 ms
Fragment duration (T_{F})	102 ms

where n_{pre} and β are the numbers of preamble symbols and of additional frame delimiter symbols used for synchronization. Let us remark that selecting the appropriate LoRa-CSS SF in DtS communications is influenced by various factors, including the Doppler effect. It was shown that the resilience of LoRa-CSS to the effects of Doppler rate and shift is closely tied to the combination of employed SF and bandwidth [36]. Specifically, SFs up to 10 have been found to offer sufficient robustness for packet demodulation during typical LEO satellite passes, while higher SFs often lack this robustness. Thus, numerical results in this section are presented for SFs 7 and 10 [11], [36].

Next, since the asynchronous frequency-hopping access model addressed in Section IV is built upon LR-FHSS transmission, we evaluated the time-on-air necessary for the transmission of an LR-FHSS frame containing PL payload data bytes as follows. The time-on-air for LR-FHSS depends on the number of header replicas and payload fragments and is $T=N_HT_H+N_FT_F$. The number of fragments depends on the payload size and on the coding rate CR and is given by

$$N_F=\left\lceil\frac{\mathrm{PL}+2}{M}\right\rceil \tag{36}$$

where $M=2$ with CR = 1/3, and $M=4$ with CR = 2/3 [16]. A comprehensive list of the simulation parameters, which have been set consistently with [3], [16], [35], and [36] is given in Table I. In the following sections, the results of the simulations are compared to the analytical models proposed in Sections III and IV. We consider a circular spot shape such that the position of the reference node varies from $(0,0)$ to $(a_{\max},0)$, where $a_{\max}=\sqrt{L^2-v^2T^2}$.

B. Probability of No Uplink Collision Over the Asynchronous Single-Frequency Channel

We start by verifying Theorem 1 by comparison with Monte Carlo simulations results. Fig. 4 shows the probability of no interference obtained by (4) versus the average number of interferers in the region $\mathcal{R}$ for a DtS LoRaWAN-based network employing LoRa-CSS with SF = 7, BW = 125 kHz, and $R=1$; it also shows the corresponding simulation results.

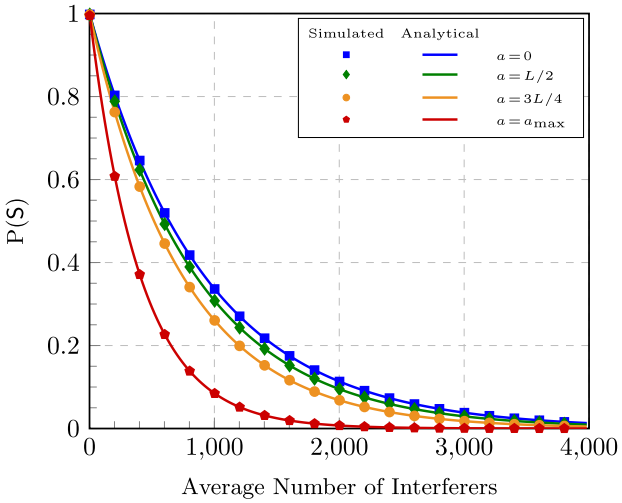

Fig. 4. Simulated and analytical probability of no interference over the single-frequency asynchronous channel (e.g., LoRa-CSS-based LoRaWAN) varying the average number of interferers.

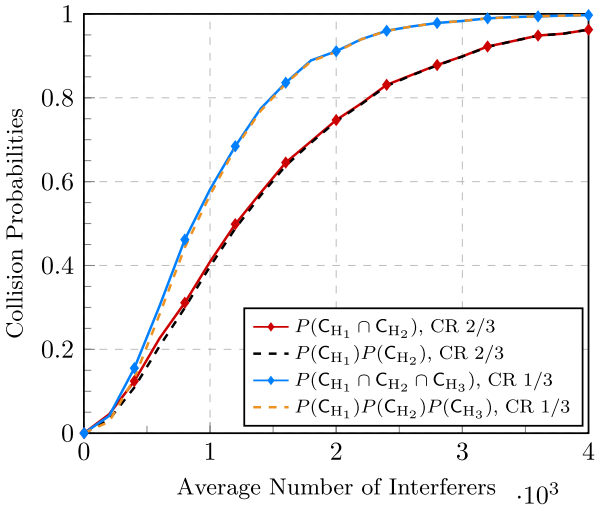

Fig. 5. Simulated joint probabilities of interference of the headers of the reference node and the products of the respective marginal probabilities, for $N_H = 2, 3$, varying the average number of interferers.

The figure highlights perfect match between analysis and simulation. As expected, the probability of no interference decreases when moving the reference node toward the border of the spot shape. This is due to the fact that, when a increases, the valid ToA range for the reference node decreases, as well as the area of the region $\mathcal{R}$. For a given average number of interferers in $\mathcal{R}$, this makes the probability $P(\mathsf{S})$ higher when the reference node is closer to the y-axis (a close to 0). It is noted that the success probability exceeds 0.9 only when the average number of interferers is less than 100.

C. Probability of No Uplink Collision Over Asynchronous Frequency-Hopping Channel (LR-FHSS)

In this section, we assess the accuracy of the analytical model expressed by Theorem 2 and the tightness of the derived upper bound. Positive correlation between the different interference events, affecting the LR-FHSS headers transmitted by the reference node, is a necessary condition in Theorem 2. We now show via numerical simulations that this condition holds for the parameter configurations adopted in this work. Fig. 5 displays the joint probabilities of interference of the headers of the reference node and the products of the respective marginal probabilities, for $N_H \in \{2, 3\}$, as a function of the average number of interferers. It can be seen that (14) holds, since the joint probability is always larger than or equal to the product of the marginals. Moreover, when the average number of interferers is large the two probabilities tend to converge, which suggests that in that case the events can be considered as almost independent.

Figs. 6 and 7 show the simulated and analytical probabilities of no interference for DtS LR-FHSS-based networks with coding rates CR $= 1/3$ and CR $= 2/3$, versus the average number of interferers in the region $\mathcal{R}$. The configurations foreseen by the LR-FHSS standard are also compared for different numbers of available OBW channels, $B \in \{35, 60, 86\}$, and for different positions of the reference node, for a payload size of 100 bytes. The figures illustrate how the analytical

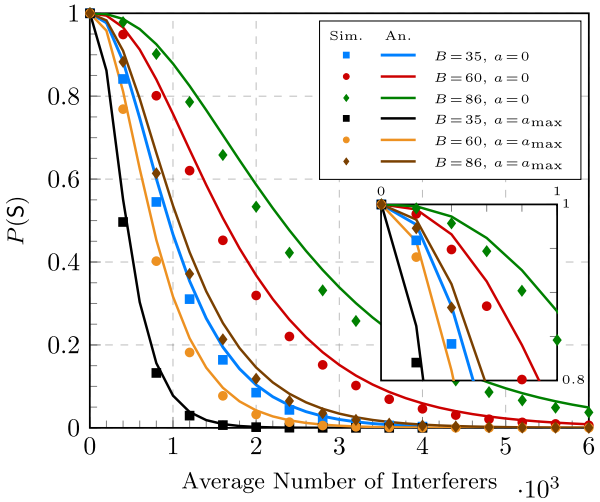

Fig. 6. Simulated and analytical success probabilities for LR-FHSS access scheme varying the average number of interferers for CR 1/3.

model bounds from above the results obtained via simulations, and how the bound is tighter when the number of available hopping channels is low (e.g., $B = 35$). Again, the probability $P(\mathsf{S})$ decreases when moving the reference node toward the border of the spot shape, as expected. Moreover, increasing the number of OBW channels available for frequency hopping translates into a remarkable increase in the system uplink capacity, i.e., the number of devices simultaneously transmitting a packet during the satellite contact time for the same probability of no interference. For example, for a target $P(\mathsf{S}) = 0.8$, LR-FHSS supports up to 600, 1000, and 1600 uplink devices transmitting 100 bytes with CR 2/3 and 35, 60, and 86 available OBWs, respectively.

D. LoRa-CSS Versus LR-FHSS: A Comparison

This section provides a comparison between LoRa-CSS and LR-FHSS uplink capacities with the aim of highlighting their strengths and weaknesses in the context of LEO

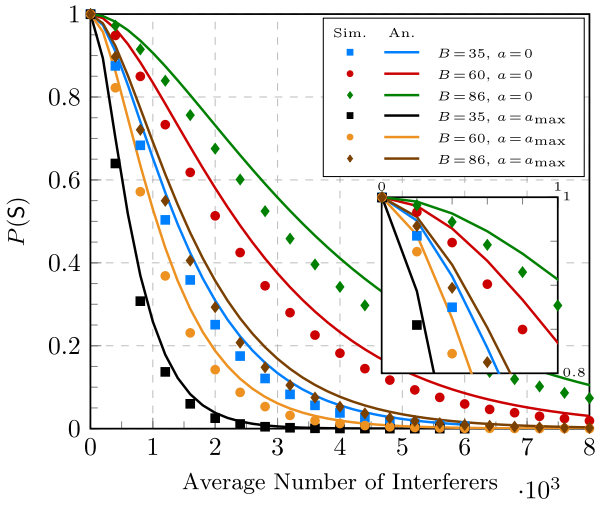

Fig. 7. Simulated and analytical success probabilities for LR-FHSS varying the average number of interferers for CR 2/3.

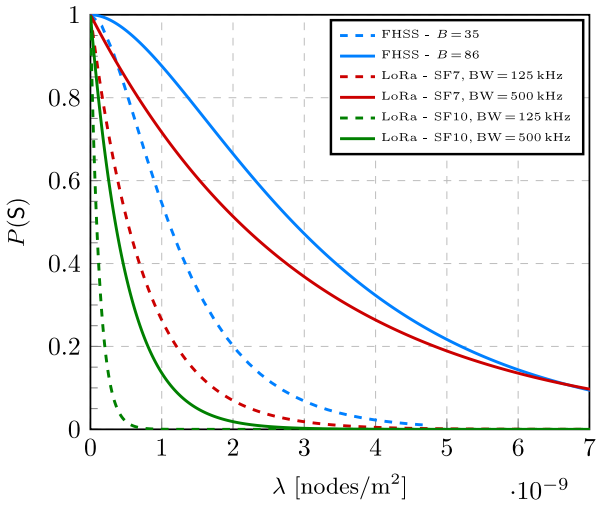

Fig. 8. Success probability for LoRa-CSS and LR-FHSS varying the density of interferers in the area.

satellite IoT applications. Fig. 8 shows the success probabilities evaluated through the analytical models proposed in Sections III and IV, varying the density of interferers in the area spanned by the satellite. The results are obtained with PL = 58 bytes, considering SFs 7 and 10, and bandwidths 125 and 500 kHz for LoRa-CSS, while CR 2/3 and $N_H = 2$ for LR-FHSS. It is evident how LR-FHSS scheme shows better performance than traditional LoRa-CSS in terms of uplink capacity. In fact, the number of nodes that can concur in the transmission of their packets during a satellite pass is larger when adopting the frequency hopping and fragmentation characteristic of LR-FHSS. We also remark that such results are obtained considering a single LoRa-CSS channel and a single-frequency-hopping grid of an LR-FHSS channel. Thus, uplink capacity can be boosted by the use of a large number of orthogonal channels, forLoRa-CSS, and frequency grids, for LR-FHSS, which potentially add a multiplicative factor to the outcomes of our simulations [16], [37], [38]. Finally, a comparison between the two most promising parameter

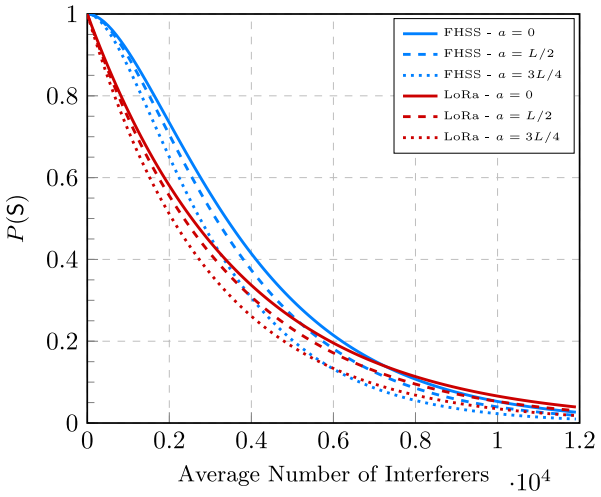

Fig. 9. Success probability for LoRa-CSS and LR-FHSS varying the average number of interferers.

settings for LR-FHSS and LoRa-CSS in terms of success probability versus the average number of interferers in the area is provided in Fig. 9. As expected, LR-FHSS achieves the best performance even when the reference device is placed near the boundary of the spot (e.g., $a = 3L/4$).

VII. Conclusion

We have investigated the probability of no uplink collision among uncoordinated devices in LEO satellite IoT. We have derived its analytical expression for unconfirmed ALOHA over a single channel (e.g., LoRaWAN class A with LoRa-CSS modulation), and an upper bound on it for unconfirmed ALOHA with frequency-hopping compliant with LR-FHSS. For this latter scheme, we have not assumed independence among collision events of packet fragments. The obtained expressions reveal the explicit dependence on the satellite velocity, the spot size, the node density on ground, and the packet time-on-air, and are independent of the satellite spot shape, provided it fulfills the explained conditions. Extensive numerical results have been performed to validate the analytical expressions. While there is perfect match in the single-frequency case, the LR-FHSS upper bound proves to be tighter when the number of channels available for frequency hopping is low (e.g., 35). A comparison between the uplink capacities of LoRa-CSS and LR-FHSS in the LEO DtS context has revealed how LR-FHSS can remarkably increase the number of devices simultaneously transmitting during the satellite pass.

Appendix A
Sum-Rate Maximization Over the Asynchronous Single-Frequency Collision Channel

In this Appendix, a closed-form expression for the sum-rate of DtS-IoT based on unconfirmed ALOHA over the asynchronous single-frequency collision channel is derived. Assume that each device transmits K information bits, such that the number of transmitted symbols can be expressed as $N_s = K\delta + \mu$, where δ depends on channel coding and

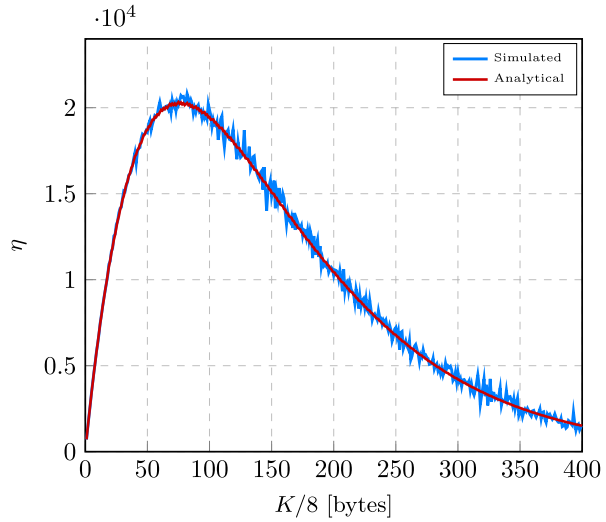

Fig. 10. Simulated and analytical sum-rate varying the number of transmitted information bits K for $\lambda = 7.13 \cdot 10^{-10}$.

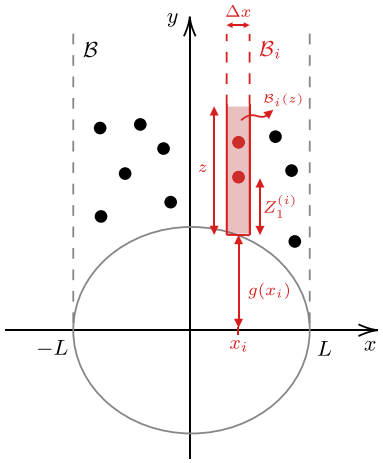

Fig. 11. Illustration of the region $\mathcal{B}$ and its partition regions $\mathcal{B}_i$. The satellite spot moves along the positive y-axis direction with constant velocity v and is centered in the origin at $t = 0$.

modulation, and μ is the overhead due to physical header, preamble, and synchronization symbols. Each symbol has duration T_s, such that $T = N_s T_s = (K\delta + \mu)T_s$. We can define the sum-rate $\eta = \eta(\lambda, K)$ as the average number of information bits received by the satellite in a time window of size $2g(0)/v$, i.e.,

$$\eta(\lambda, K) = K\lambda A_{\mathcal{R}} P(\mathsf{S}) = K\lambda A_{\mathcal{R}} e^{-4Lv\lambda(K\delta+\mu)T_s}. \quad (37)$$

The parameters λ and K can be chosen to maximize η, i.e.,

$$\{\lambda^\star, K^\star\} = \arg\max_{\lambda,K} \eta(\lambda, K). \quad (38)$$

From (38), it follows directly that

$$\lambda^\star K^\star = \frac{1}{4Lv\delta T_s}. \quad (39)$$

Incorporating (39) in (37) yields the maximum sum-rate

$$\eta_{\max} = \eta(\lambda^\star, K^\star) = \frac{A_{\mathcal{R}}}{4Lv\delta T_s e} e^{-4Lv\lambda^\star \mu T_s}. \quad (40)$$

Fig. 10 shows the sum-rate varying the number of transmitted information bits for $\lambda = 7.13 \cdot 10^{-10}$, highlighting perfect match between analysis and simulation. The results are obtained considering a DtS LoRaWAN-based network with SF = 7, BW = 125 kHz, and $R = 1$.

Appendix B
Alternative Proof of Theorem 1

In the following, we provide an alternative proof for Theorem 1 showing that the packet arrival process at the satellite, when the nodes are distributed on ground according to a PPP and the satellite spot does not initially contain any node, is an inhomogeneous Poisson process that becomes homogeneous with rate $\rho = 2Lv\lambda$ [packets/s] when the system reaches steady state. Let us denote by $\mathcal{B} \subset \mathbb{R}^2$ the region swept by the upper boundary of the satellite spot from $t = 0$ onward, as illustrated in Fig. 11.[2] Let us partition the interval $[-L, L]$ on the x-axis into $2L/\Delta x$ intervals, each of size Δx. We take Δx small and later we will let Δx tend to zero. Let x_i be the center of the ith such interval and $\mathcal{B}_i$ be the corresponding partition region. We order the nodes in $\mathcal{B}_i$, indexing them with $k \geq 1$, based on their increasing distance from the boundary of the satellite spot at time $t = 0$. We denote by $Z_k^{(i)}$ the random variable representing the distance of node k in $\mathcal{B}_i$ from such a boundary ($Z_1^{(i)}$ is shown in Fig. 11). We also denote by $\mathcal{B}_i(z)$ the rectangular region $[(i-1)\Delta x, i\Delta x] \times [g(x_i), g(x_i) + z]$ and by $Q_i(z)$ the number of nodes in $\mathcal{B}_i(z)$. The cumulative distribution function (CDF) of $Z_k^{(i)}$ is

$$P\left(Z_k^{(i)} \leq z\right) = P(Q_i(z) \geq k) = \sum_{l=k}^{\infty} \frac{(\lambda \Delta x z)^l}{l!} e^{-\lambda \Delta x z}. \quad (41)$$

Thus, under the assumption that the spatial distribution of nodes is a PPP, $Z_k^{(i)}$ is Erlang distributed, as $\text{Erlang}(z; k, \lambda\Delta x)$.

Next, let us denote by $\Theta_k^{(i)}$ the start contact time of node k, i.e., $\Theta_k^{(i)} = Z_k^{(i)}/v \sim \text{Erlang}(\theta; k, \lambda v \Delta x)$. Let us also denote: by $A_j^{(i)}$ the jth packet arrival time from nodes in $\mathcal{B}_i$; by $N_i(t)$ the number of packet arrivals from the nodes in $\mathcal{B}_i$ before time t; and by $M_i(t)$ the number of devices in $\mathcal{B}_i$ entered into the satellite spot before time t. The CDF of $A_j^{(i)}$ can be expressed as

$$\begin{aligned} P\left(A_j^{(i)} \leq t\right) &= P(N_i(t) \geq j) \\ &= \sum_{n=j}^{\infty} P(N_i(t) = n) \\ &= \sum_{n=j}^{\infty} \sum_{m=n}^{\infty} P(N_i(t) = n | M_i(t) = m) P(M_i(t) = m). \end{aligned} \quad (42)$$

From basic properties of Poisson arrival processes, given that $M_i(t) = m$, the contact times are independent and uniformly distributed, i.e., given that $M_i(t) = m$ we have $\Theta_k^{(i)} \sim \mathcal{U}(0, t)$.

[2] As mentioned, we assume that at time $t = 0$ the satellite spot is empty, i.e., no device has entered the spot yet.

The ToA of the packet from the kth device in $\mathcal{B}_i$ is therefore $S_k^{(i)} = \Theta_k^{(i)} + D_k^{(i)}$ where $D_k^{(i)} \sim \mathcal{U}(0, \delta_i)$ and $\delta_i = [2g(x_i)/v] - T$.[3] The conditional PDF of $S_k^{(i)}$ given $M_i(t) = m$ is the convolution of the two uniform distributions, namely

$$f_{\S_k^{(i)}|M_i(t)}(z|m) = \int_{-\infty}^{\infty} f_{\Theta_k^{(i)}|M_i(t)}(\xi|m) f_{D_k^{(i)}}(z-\xi)\mathrm{d}\xi = \begin{cases} 0, & \text{if } z < 0 \\ \frac{z}{\delta_i t}, & \text{if } 0 \le z \le \delta_i \\ \frac{1}{t}, & \text{if } \delta_i < z \le t \\ \frac{t-(z-\delta_i)}{\delta_i t}, & \text{if } t < z \le t+\delta_i \\ 0, & \text{if } z > t+\delta_i \end{cases} \tag{43}$$

from which we obtain

$$P\left(\S_k^{(i)} \le t | M_i(t) = m\right) = 1 - \frac{\delta_i}{2t}. \tag{44}$$

Therefore, it follows that:

$$P(N_i(t) = n | M_i(t) = m) = \binom{m}{n}\left(1 - \frac{\delta_i}{2t}\right)^n \left(\frac{\delta_i}{2t}\right)^{m-n}. \tag{45}$$

Let us define $\mu_i = \lambda v \Delta x$. Incorporating (45) into (42) yields

$$\begin{aligned} P\left(A_j^{(i)} \le t\right) &= \sum_{n=j}^{\infty}\sum_{m=n}^{\infty}\binom{m}{n}\left(1-\frac{\delta_i}{2t}\right)^n\left(\frac{\delta_i}{2t}\right)^{m-n}\frac{(\mu_i t)^m}{m!}e^{-\mu_i t} \\ &= e^{-\mu_i t}\sum_{n=j}^{\infty}\frac{\left(\mu_i t - \frac{\delta_i\mu_i}{2}\right)^n}{n!}\sum_{m=n}^{\infty}\frac{\left(\frac{\delta_i\mu_i}{2}\right)^{m-n}}{(m-n)!} \\ &= \sum_{n=j}^{\infty}\frac{\left(\left(\mu_i - \frac{\delta_i\mu_i}{2t}\right)t\right)^n}{n!}e^{-\left(\mu_i - \frac{\delta_i\mu_i}{2t}\right)t}. \end{aligned} \tag{46}$$

Recalling that $P(A_j^{(i)} \le t) = P(N_i(t) \ge j)$, (46) shows that the process governing packet arrivals at the satellite is a nonhomogeneous Poisson process [39]. Nonetheless, as t increases, the process reaches a steady-state condition where it becomes homogeneous with rate μ_i [packets/s]. Considering the steady state, the superposition of the $2L/\Delta x$ independent packet arrival Poisson processes is a Poisson process whose rate is the sum of the rates of the merged processes. Letting $\Delta x \to 0$ (a regime under which the analysis is exact) we obtain

$$\begin{aligned} \rho &= \lim_{\Delta x \to 0}\sum_{i=1}^{2L/\Delta x}\mu_i = v\lambda\int_{-L}^{L}1\mathrm{d}x \\ &= 2Lv\lambda. \end{aligned} \tag{47}$$

The proof is concluded by noting that (4) is the probability that no interfering packet arrives at the satellite in a time window of duration $2T$ (vulnerability period), yielding

$$P(\mathsf{S}) = e^{-2T\rho} = e^{-4LT v\lambda}. \tag{48}$$

ACKNOWLEDGMENT

The authors would like to thank the anonymous reviewers and the associate editor for their comments which helped to improve this article.

[3]Recall from Section II that, at every pass, each node sets the ToA of its packet by drawing a uniform random variable in its valid ToA range.

REFERENCES

[1] E. Testi and E. Paolini, "Packet collision probability analysis in contention-based direct-to-satellite IoT uplink," presented at the IEEE Int. Symp. Pers. Indoor Mob. Radio Commun., Valencia, Spain, Sep. 2024.

[2] O. Kodheli, N. Maturo, S. Chatzinotas, S. Andrenacci, and F. Zimmer, "NB-IoT via LEO satellites: An efficient resource allocation strategy for uplink data transmission," *IEEE Internet Things J.*, vol. 9, no. 7, pp. 5094–5107, Aug. 2022.

[3] M. Centenaro, C. E. Costa, F. Granelli, C. Sacchi, and L. Vangelista, "A survey on technologies, standards and open challenges in satellite IoT," *IEEE Commun. Surveys Tuts.*, vol. 23, no. 3, pp. 1693–1720, 3rd Quart., 2021.

[4] J. Jiao, S. Wu, R. Lu, and Q. Zhang, "Massive access in space-based Internet of Things: Challenges, opportunities, and future directions," *IEEE Wireless Commun.*, vol. 28, no. 5, pp. 118–125, Oct. 2021.

[5] J. Fraire, S. Céspedes, and N. Accettura, "Direct-to-satellite IoT—A survey of the state of the art and future research perspectives: Backhauling the IoT through LEO satellites," in *Proc. 18th Int. Conf. Ad-Hoc Netw. Wireless*, Oct. 2019, pp. 241–258.

[6] A. A. Doroshkin, A. M. Zadorozhny, O. N. Kus, V. Y. Prokopyev, and Y. M. Prokopyev, "Experimental study of lora modulation immunity to doppler effect in CubeSat radio communications," *IEEE Access*, vol. 7, pp. 75721–75731, 2019.

[7] Z. Qu, G. Zhang, H. Cao, and J. Xie, "LEO satellite constellation for Internet of Things," *IEEE Access*, vol. 5, pp. 18391–18401, 2017.

[8] S. K. Routray, R. Tengshe, A. Javali, S. Sarkar, L. Sharma, and A. D. Ghosh, "Satellite based IoT for mission critical applications," in *Proc. Int Conf. Data Sci. Commun.*, Mar. 2019, pp. 1–6.

[9] V. Almonacid and L. Franck, "Extending the coverage of the Internet of Things with low-cost nanosatellite networks," *Acta Astronautica*, vol. 138, pp. 95–101, Sep. 2017.

[10] I. F. Akyildiz and A. Kak, "The Internet of Space Things/CubeSats," *IEEE Netw.*, vol. 33, no. 5, pp. 212–218, Sep. 2019.

[11] G. Álvarez, J. A. Fraire, K. A. Hassan, S. Céspedes, and D. Pesch, "Uplink transmission policies for LoRa-based direct-to-satellite IoT," *IEEE Access*, vol. 10, pp. 72687–72701, 2022.

[12] M. A. Ullah, A. Yastrebova, K. Mikhaylov, M. Höyhtyä, and H. Alves, "Situational awareness for autonomous ships in the arctic: mMTC direct-to-satellite connectivity," *IEEE Commun. Mag.*, vol. 60, no. 6, pp. 32–38, Jun. 2022.

[13] T. Ferrer, S. Céspedes, and A. Becerra, "Review and evaluation of MAC protocols for satellite IoT systems using nanosatellites," *Sensors*, vol. 19, no. 8, p. 1947, Apr. 2019.

[14] (Sigfox, Toulouse, France). *Sigfox Connected Objects: Radio Specifications, Reference EPSPECS V1.7*. May 2023. [Online]. Available: https://build.sigfox.com/sigfox-device-radio-specifications

[15] G. Boquet, P. Tuset-Peiró, F. Adelantado, T. Watteyne, and X. Vilajosana, "LR-FHSS: Overview and performance analysis," *IEEE Commun. Mag.*, vol. 59, no. 3, pp. 30–36, Mar. 2021.

[16] (LoRa Alliance, Fremont, CA, USA). *RP002-1.0.2 LoRaWAN® Regional Parameters*. 2020. [Online]. Available: https://lora-alliance.org/resource_hub/rp2-102-lorawan-regional-parameters/

[17] N. Abramson, "THE ALOHA SYSTEM: Another alternative for computer communications," in *Proc. Fall Joint Comput. Conf.*, Nov. 1970, pp. 281–285.

[18] L. Kleinrock and S. Lam, "Packet switching in a multiaccess broadcast channel: Performance evaluation," *IEEE Trans. Commun.*, vol. 23, no. 4, pp. 410–423, Apr. 1975.

[19] G. Choudhury and S. Rappaport, "Diversity ALOHA—A random access scheme for satellite communications," *IEEE Trans. Commun.*, vol. 31, no. 3, pp. 450–457, Mar. 1983.

[20] O. del Rio Herrero, G. Foti, and G. Gallinaro, "Spread-spectrum techniques for the provision of packet access on the reverse link of next-generation broadband multimedia satellite systems," *IEEE J. Sel. Areas Commun.*, vol. 22, no. 3, pp. 574–583, Apr. 2004.

[21] E. Casini, R. De Gaudenzi, and O. del Rio Herrero, "Contention resolution diversity slotted ALOHA (CRDSA): An enhanced random access scheme for satellite access packet networks," *Front. Space Technol.* vol. 6, no. 4, pp. 1408–1419, Apr. 2007.

[22] J. B. Eom and T.-J. Lee, "Accurate tag estimation for dynamic framed-slotted ALOHA in RFID systems," *IEEE Commun. Lett.*, vol. 14, no. 1, pp. 60–62, Jan. 2010.

[23] H. Jiang et al., "Enabling LPWAN massive access: Grant-free random access with massive MIMO," *IEEE Wireless Commun.*, vol. 29, no. 4, pp. 72–77, Aug. 2022.

[24] Y. Qin, M. A. Kishk, and M.-S. Alouini, "Stochastic-geometry-based analysis of multipurpose UAVs for package and data delivery," *IEEE Internet Things J.*, vol. 10, no. 5, pp. 4664–4676, Mar. 2023.
[25] Y. Qin, M. A. Kishk, and M.-S. Alouini, "On the peak AoI of UAV-assisted IoT networks: A stochastic geometry approach," *IEEE Internet Things J.*, vol. 11, no. 5, pp. 8676–8689, Mar. 2024.
[26] A. Talgat, M. A. Kishk, and M.-S. Alouini, "Stochastic geometry-based analysis of LEO satellite communication systems," *IEEE Commun. Lett.*, vol. 25, no. 8, pp. 2458–2462, Oct. 2021.
[27] A. Talgat, M. A. Kishk, and M.-S. Alouini, "Stochastic geometry-based uplink performance analysis of IoT over LEO satellite communication," *IEEE Trans. Aerosp. Electron. Syst.*, vol. 60, no. 4, pp. 4198–4213, Aug. 2024.
[28] J. A. Fraire, S. Henn, F. Dovis, R. Garello, and G. Taricco, "Sparse satellite constellation design for LoRa-based direct-to-satellite Internet of Things," in *Proc. IEEE Global Commun. Conf.*, Dec. 2020, pp. 1–16.
[29] W. Zhou, T. Hong, X. Ding, and G. Zhang, "LoRa performance analysis for LEO satellite IoT networks," in *Proc. Int. Conf. Wireless Commun. Signal Process.*, Changsha, China, Oct. 2021, pp. 1–5.
[30] A. Maleki, H. H. Nguyen, and R. Barton, "Outage probability analysis of LR-FHSS in satellite IoT networks," *IEEE Commun. Lett.*, vol. 27, no. 3, pp. 946–950, Mar. 2023.
[31] M. A. Ullah, K. Mikhaylov, and H. Alves, "Analysis and simulation of LoRaWAN LR-FHSS for direct-to-satellite scenario," *IEEE Wireless Commun. Lett.*, vol. 11, no. 3, pp. 548–552, Mar. 2022.
[32] D. A. Dawson and D. Sankoff, "An inequality for probabilities," *Proc. Amer. Math. Soc.*, vol. 18, no. 3, pp. 504–507, Jun. 1967.
[33] C. Bonferroni, *Teoria Statistica Delle Classi e Calcolo Delle Probabilità*, (Pubblicazioni del R. Istituto Superiore di Scienze Economiche e Commerciali di Firenze), vol. 8. Firenze, Italy: Seeber, 1936.
[34] E. Testi and E. Paolini. "Monte Carlo simulator for packet collision probability of direct-to-satellite IoT systems." GitHub. 2024. [Online]. Available: https://github.com/wilabcnit/wilablpwanntnsim
[35] N. Sornin and A. Yegin. "LoRaWAN specification." Accessed: Jun. 17, 2022. [Online]. Available: https://https://lora-alliance.org/wp-content/uploads/2020/11/lorawan1.0.3.pdf
[36] M. A. Ullah, G. Pasolini, K. Mikhaylov, and H. Alves, "Understanding the limits of LoRa direct-to-satellite: The Doppler perspectives," *IEEE Open J. Commun. Soc.*, vol. 5, pp. 51–63, 2024.
[37] M. Chiani and A. Elzanaty, "On the LoRa modulation for IoT: Waveform properties and spectral analysis," *IEEE Internet Things J.*, vol. 6, no. 5, pp. 8463–8470, Oct. 2019.
[38] D. Croce, M. Gucciardo, S. Mangione, G. Santaromita, and I. Tinnirello, "Impact of LoRa imperfect orthogonality: Analysis of link-level performance," *IEEE Commun. Lett.* vol. 22, no. 4, pp. 796–799, Jan. 2018.
[39] J. F. C. Kingman, *Poisson Processes*. Oxford, U.K.: Clarendon Press, 1993.

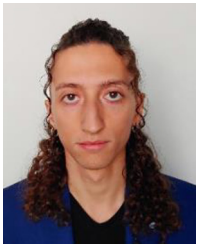

Enrico Testi (Member, IEEE) received the M.S. degree (magna cum laude) in electronics and telecommunications engineering for energy and the Ph.D. degree in electronics, telecommunications, and information technologies engineering from the University of Bologna, Bologna, Italy, in 2018 and 2022, respectively.

He is currently a Junior Assistant Professor with the Department of Electrical, Electronic, and Information Engineering "Guglielmo Marconi," University of Bologna, Cesena, Italy. He has been affiliated with the National Laboratory of Wireless Communications (WiLab) of the Italian National Inter-University Consortium for Telecommunications since 2020. His research interests include artificial intelligence techniques for next-generation wireless networks, massive MIMO, and satellite IoT.

Dr. Testi is also the Secretary/Treasurer of the IEEE ITSoc Italy Section Chapter.

Enrico Paolini (Senior Member, IEEE) received the Dr.Ing. degree (summa cum laude) in telecommunications engineering and the Ph.D. degree in electrical engineering from the University of Bologna, Bologna, Italy, in 2003 and 2007, respectively.

While working toward the Ph.D. degree, he was a Visiting Research Scholar with the Department of Electrical Engineering, University of Hawai'i at Manoa, Honolulu, HI, USA. He was a Visiting Scientist with the Institute of Communications and Navigation, German Aerospace Center, Wessling, Germany, in 2012 and 2014, under DLR-DAAD fellowships. He is currently an Associate Professor with the Department of Electrical, Electronic, and Information Engineering, University of Bologna, Cesena, Italy. His research interests include digital communication systems, error-correcting codes, massive multiple access protocols, joint sensing, and communications.

Dr. Paolini served as the Co-Chair for the ICC 2014, ICC 2015, and ICC 2016 Workshop on Massive Uncoordinated Access Protocols (MASSAP), the VTC 2019-Fall Workshop on Small Data Networks, the 2018 IEEE European School of Information Theory, and the 2020 IEEE Information Theory Workshop. He served as the TPC Co-Chair for the IEEE GLOBECOM 2022—Communication Theory Symposium and the IEEE GLOBECOM 2019—Communication Theory Symposium. He is a past Chair of the ITSoc Italy Section Chapter and the Vice-Chair of the IEEE ComSoc Radio Communications Committee. He was an Editor of IEEE COMMUNICATIONS LETTERS from 2012 to 2015 and the IEEE TRANSACTIONS ON COMMUNICATIONS (in coding and information theory) from 2015 to 2020.

Open Access funding provided by 'Alma Mater Studiorum - Università di Bologna' within the CRUI CARE Agreement